[Stefan J. Wijnholds, Sebastiaan van der Tol,
Ronald Nijboer, and Alle-Jan van der Veen]

© PHOTODISC

Calibration Challenges for Future Radio Telescopes

[An overview of a daunting parameter-estimation task]

Instruments for radio astronomical observations have come a long way. While the first telescopes were based on very large dishes and two-antenna interferometers, current instruments consist of dozens of steerable dishes, whereas future instruments will be even larger distributed sensor arrays with a hierarchy of phased array elements. For such arrays to provide meaningful output (images), accurate calibration is of critical importance. Calibration must solve for the unknown antenna gains and phases as well as the unknown atmospheric and ionospheric disturbances. Future telescopes will have a large number of elements and a large field of view (FOV). In this case, the parameters are strongly direction-dependent, resulting in a large number of unknown parameters, even if appropriately constrained physical or phenomenological descriptions are used. This makes calibration a daunting parameter-estimation task.

INTRODUCTION

Astronomers study the physical phenomena outside the Earth's atmosphere by observing cosmic particles and electromagnetic waves impinging on the Earth. Each type of observation provides another perspective on the Universe thereby unraveling some mysteries while raising new questions. Over the years, astronomy has become a true multi-wavelength science. A nice demonstration is provided in Figure 1. In this figure, the neutral hydrogen gas observed with the Westerbork synthesis radio telescope (WSRT) exhibits an intricate extended structure that is completely invisible in the optical image from the Sloan digital sky survey [1]. The radio observations therefore provide a radically different view on the dynamics of this galaxy.

Images like Figure 1 are only possible if the instruments used to observe different parts of the electromagnetic spectrum provide a similar resolution. This poses quite a challenge since the resolution of any telescope is determined by the ratio of the

Digital Object Identifier 10.1109/MSP.2009.934853

1053-5888/10/$26.00©2010IEEE

wavelength and the telescope diameter. Consequently, the aperture of radio telescopes has to be five to six orders of magnitude larger than that of an optical telescope to provide comparable resolution, i.e., radio telescopes should have an aperture of several hundreds of kilometers. Although it is not feasible to make a dish of this size, it is possible to synthesize an aperture by building an interferometer, i.e., an array.

Radio astronomy began at Bell Telephone Laboratories with Karl Jansky's 1928 discovery that the source of unwanted interference in his short-wave radio transmissions actually came from the Milky Way. For this, he used the large antenna mounted on a turntable shown in Figure 2(a). Subsequent single-antenna instruments were based on increasingly larger dishes, culminating in the Arecibo telescope (Puerto Rico, 1960, 305 m nonsteerable dish) and the Effelsberg telescope (Bonn, Germany, 1972, 100 m steerable dish [Figure 2(b)]). Making larger steerable dishes is not practical.

An interferometer measures the correlation between two antennas spaced at a certain distance. Initially used to study a single source passing over the sky, the principle was used in optical astronomy in the Michelson stellar interferometer (1890 and 1920); the first radio observations using two dipoles were done by Ryle and Vonberg in 1946 [3]. Examples of subsequent instruments are as follows:

- the Cambridge one-mile telescope in Cambridge, United Kingdom (1964, two fixed and one movable 18.3 m dishes)
- the 3 km WSRT in Westerbork, The Netherlands [1970, 12 fixed and two movable 25-m dishes, see Figure 2(c)]
- the 36 km very large array (VLA) in Socorro, New Mexico, United States [1980, 27 movable 25 m dishes, see Figure 2(d)]

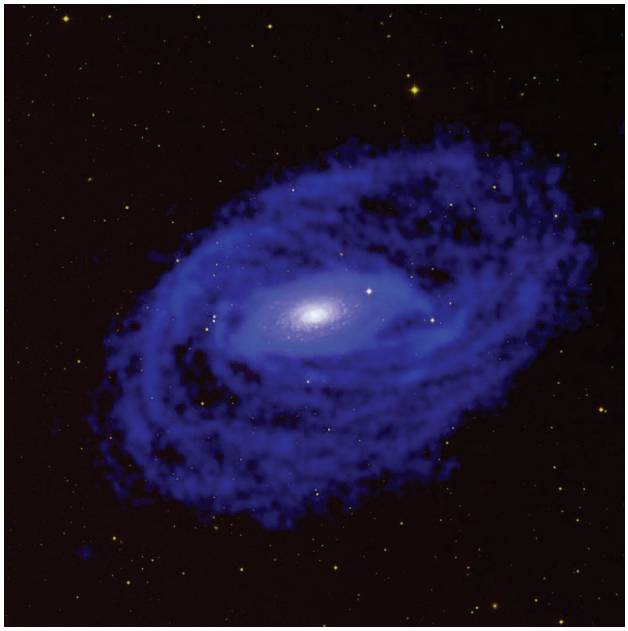

[FIG1] Image of the spiral galaxy NGC 5055, showing the structure of the neutral hydrogen gas observed with the WSRT (blue) superimposed on an optical image of the same galaxy from the Sloan digital sky survey (white) [2].

- the 25 km giant meter-wave radio telescope (GMRT) in Pune, India (1998, 30 dishes with 45 m diameter).

These telescopes use the Earth's rotation to obtain a sequence of correlations for varying antenna baseline orientations relative to the desired sky image field, resulting in high-resolution images via synthesis mapping. Even larger baselines

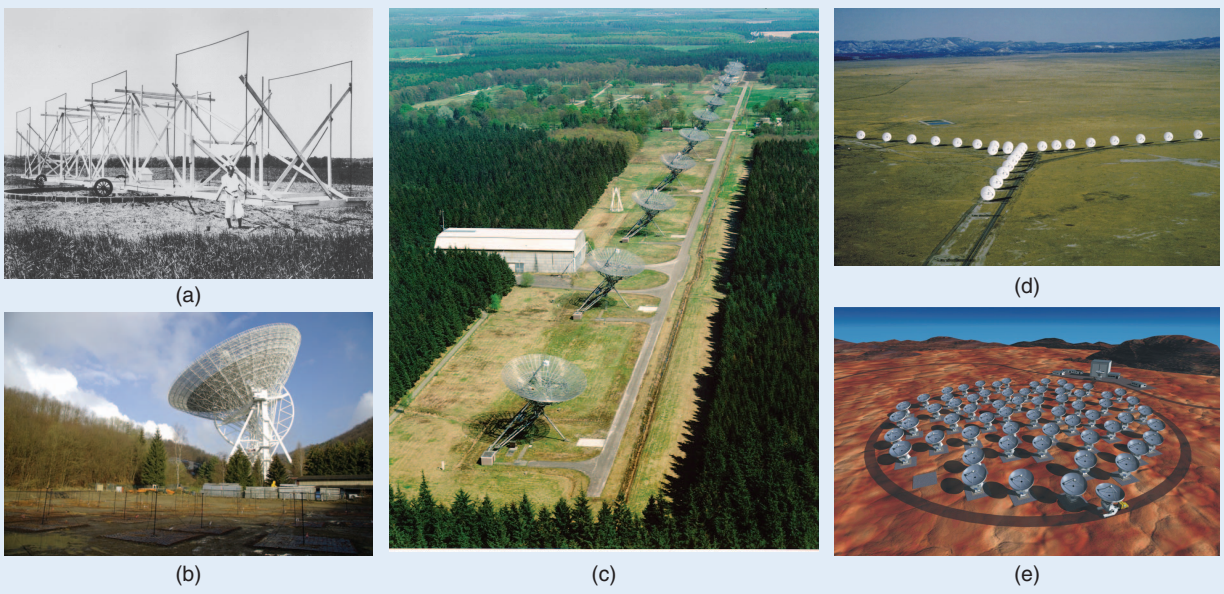

[FIG2] The radio telescopes of (a) Jansky [courtesy of National Radio Astronomy Observatory (NRAO)], (b) Effelsberg (courtesy Stefan Wijnholds), (c) WSRT [courtesy of The Netherlands Institute for Radio Astronomy (ASTRON)], (d) VLA (courtesy of NRAO), and (e) concept for ALMA (courtesy of the ALMA Observatory).

(up to a few thousand kilometers) were obtained by combining these instruments into a single instrument using a technique called very long baseline interferometry (VLBI), where the telescope outputs are time-stamped and postprocessed by correlation at a central location. An extensive historical overview is presented in [4].

OVER THE YEARS, ASTRONOMY HAS BECOME A TRUE MULTIWAVELENGTH SCIENCE.

In the near future, astronomers will have built even larger arrays, such as

- The Atacama large millimeter array (ALMA) in Chile, scheduled for completion in 2011. It will have 50 movable, 12 m dishes with possible extension to 64 dishes [see Figure 2(e)].
- The low frequency array (LOFAR) in The Netherlands, whose completion will be finished in 2010. It will have about 30,000 dipole antennas grouped in 36 stations (see Figure 3).
- The square kilometer array (SKA), which is planned to be operational in or around 2020 (see Figure 3).

The August 2009 issue of *Proceedings of the IEEE* provides overview articles discussing many of the recent and future telescopes.

High-resolution synthesis imaging would not be possible without accurate calibration. Initially, the complex antenna gains and phases are unknown; they have to be estimated. Moreover, propagation through the atmosphere and ionosphere causes additional phase delays that may create severe distortions. Finally, image reconstruction or mapmaking is governed by finite sample effects: we can only measure correlations on a small set of baselines. Solving for these three effects is intertwined and creates very interesting signal processing problems. In this article, we focus on the calibration aspects, whereas imaging is covered in a companion article [5]. The examples

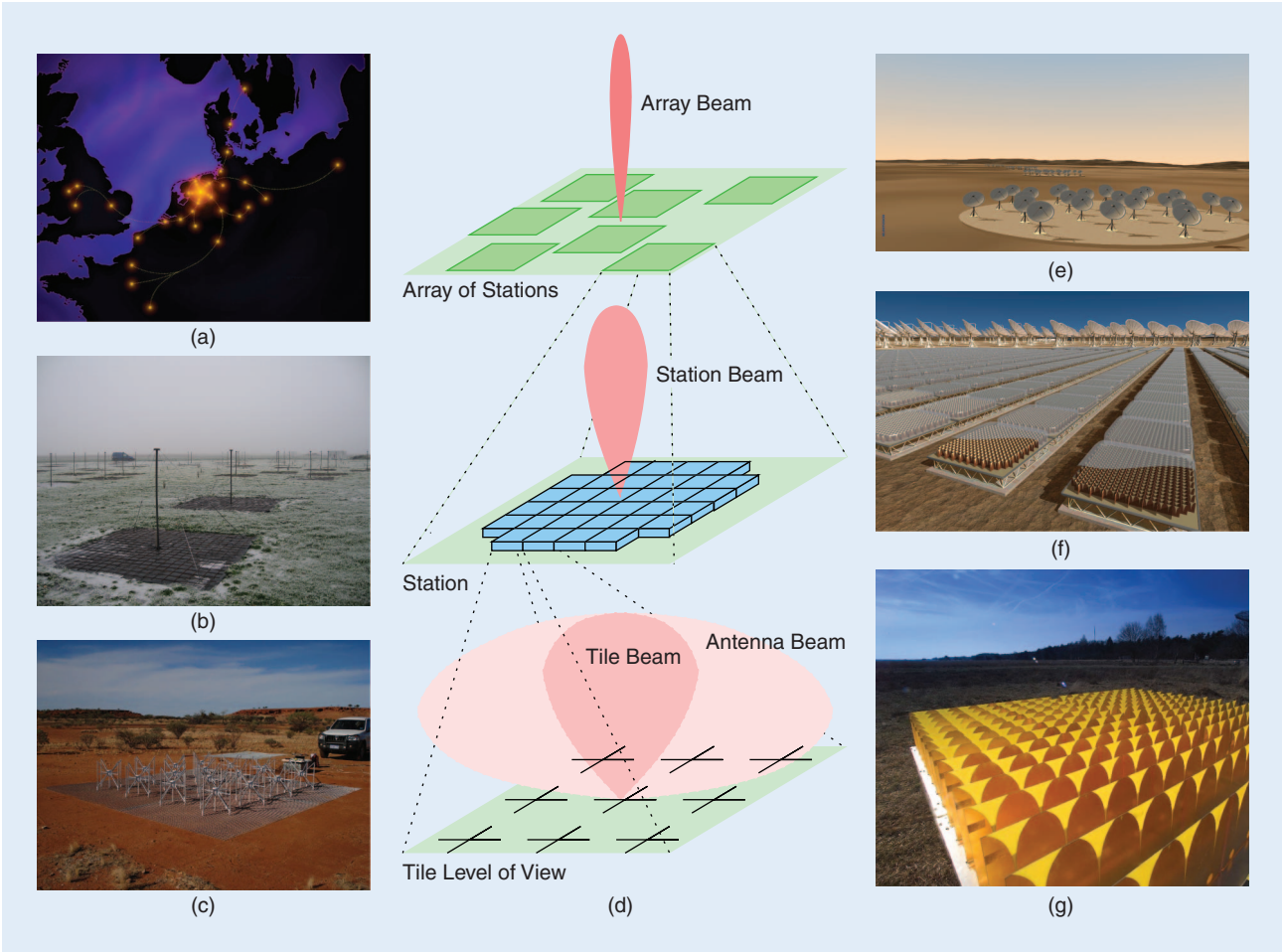

[FIG3] The schematic in the center (d) shows the beamforming hierarchy, explained in more detail in the section "Telescope Architectures," with the array beam produced by an array of stations at the top and the antenna beam at the bottom. Subsequent levels in the hierarchy have beams that are narrower and more sensitive. The different levels are illustrated by (a) the concept layout of LOFAR (image courtesy of ASTRON), (b) a LOFAR low-band antenna station (image courtesy of Menno Norden), (c) an MWA tile (image courtesy of the MWA project), (e) a concept for SKA consisting of an array of stations, each with small dishes, (f) a concept for the SKA core station (both images courtesy of the SKA project), and (g) a SKA demonstrator tile consisting of Vivaldi antennas (image courtesy of ASTRON).

provided in this article are generally borrowed from low-frequency (<1.5 GHz) instruments, but the framework presented is also applicable to high-frequency instruments like ALMA.

INTERFEROMETRY AND IMAGE FORMATION

The concept of interferometry is illustrated in Figure 4. An interferometer measures the spatial coherency of the incoming electromagnetic field. This is done by correlating the signals from the individual receivers with each other. The correlation of each pair of receiver outputs provides the amplitude and phase of the spatial coherence function for the baseline defined by the vector pointing from the first to the second receiver. These correlations are called the visibilities.

IDEAL MEASUREMENT MODEL

To describe this mathematically, (see "Notation" for notational conventions), let us assume that there are J array elements called "antennas" pointed at a field with Q point sources. As discussed in the section "Telescope Architectures," each element may be a phased array itself. Stack the sampled antenna signals for the kth narrowband [6] frequency channel centered at frequency f_k into a $J \times 1$ vector $\mathbf{x}(n)$. For notational convenience, we will drop the dependence on frequency from the notation in most of the article. Then we can model $\mathbf{x}(n)$ as

$$\mathbf{x}(n) = \sum_{q=1}^{Q} \mathbf{a}_q(n) s_q(n) + \mathbf{n}(n), \tag{1}$$

where $s_q(n)$ is the signal from the qth source at time sample n and frequency f_k, $\mathbf{a}_q(n)$ is the array response vector for this source, and $\mathbf{n}(n)$ is the noise sample vector. $s_q(n)$ and $\mathbf{n}(n)$ are baseband complex envelope representations of zero mean wide sense stationary white Gaussian random processes sampled at the Nyquist rate.

Due to the rotation of the Earth, the geometrical delay component of $\mathbf{a}_q(n)$ changes slowly with time, which is a critical feature exploited in synthesis imaging. Let N be the number of time samples in a short-term integration (STI) interval. We assume that $\mathbf{a}_q(n)$ is (relatively) constant over such an interval, so that, for the mth interval, $\mathbf{x}(n)$ is wide sense stationary over $(m-1)N \le n \le mN-1$. A single STI autocovariance is defined as

$$\mathbf{R}_m = E\{\mathbf{x}(n)\,\mathbf{x}^H(n)\} = \mathbf{A}_m \Sigma_s \mathbf{A}_m^H + \Sigma_n, \tag{2}$$

where $\mathbf{R}_m$ has size $J \times J$,

$$\begin{aligned} \mathbf{A}_m &= [\,\mathbf{a}_1((m-1)N), \ldots, \mathbf{a}_Q((m-1)N)\,] \\ \Sigma_s &= \mathrm{diag}\{[\sigma_1^2, \ldots, \sigma_Q^2]\} \\ \Sigma_n &= E\{\mathbf{n}(n)\,\mathbf{n}^H(n)\} \;=\; \mathrm{diag}\{[\sigma_{n,1}^2, \ldots, \sigma_{n,J}^2]\}. \end{aligned}$$

Here, σ_q^2 is the variance of the qth source. Noise is assumed to be independent but not evenly distributed across the array, and the noise variances $\sigma_{n,j}^2$ are unknown. With some abuse of notation, the subscript n in Σ_n and $\sigma_{n,j}$ indicates "noise."

Each matrix element of $(\mathbf{R}_m)_{ij}$ represents the interferometric correlation along the baseline vector between the antennas i and j in the array. The corresponding short term integration sample covariance estimate is

$$\hat{\mathbf{R}}_m = \frac{1}{N} \sum_{n=(m-1)N}^{mN-1} \mathbf{x}(n)\mathbf{x}^H(n),$$

and this is what the interferometer measures for subsequent processing. In practical instruments, the short-term integration interval is often in the order of 1–30 s, the total observation can span up to 12 hours, and the number of frequency bins is highly design-dependent, ranging in order of magnitude from 10 to 10^5.

Under ideal circumstances, the array response matrix $\mathbf{A}_m$ is equal to a phase matrix $\mathbf{K}_m$ due entirely to the geometrical delays associated with the array and source geometry, and accurately known, at least for the calibration sources. The columns of $\mathbf{K}_m$, denoted by $\mathbf{k}_{m,q}$ $(q = 1, \ldots, Q)$, are often called the Fourier kernel and are given by

$$\begin{aligned} \mathbf{k}_{m,q} &= \exp\left\{ -\mathrm{j}\frac{2\pi f_k}{c} \mathbf{Z}^T \mathbf{p}_{m,q} \right\} \\ \mathbf{Z} &= [\mathbf{z}_1^T, \ldots, \mathbf{z}_J^T]^T, \end{aligned}$$

where c is the speed of light, $\mathbf{z}_j$ is the position column vector for the jth array element, and $\mathbf{p}_{m,q}$ is a unit length vector pointing in the direction of source q during STI snapshot m.

NOTATION

$\otimes$	Kronecker product
$\circ$	Khatri-Rao (column-wise Kronecker) product
$\odot$	Schur (entry-wise) matrix product
$\oslash$	Entry-wise matrix division
$(\cdot)^T$	Transpose operator
$(\cdot)^H$	Hermitian (conjugate) transpose operator
$(\mathbf{A})^{\odot\beta}$	Entry-wise power of a matrix
vec$(\cdot)$	Stacking of the columns of a matrix
diag$(\cdot)$	Diagonal matrix constructed from a vector
$\overline{a}$	Complex conjugate of a
†	Moore-Penrose pseudoinverse

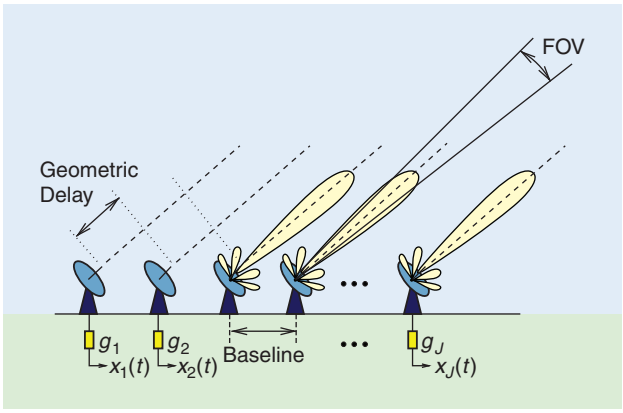

[FIG4] Schematic overview of a radio interferometer.

IMAGE FORMATION

Ignoring the additive noise, the measurement (2), in its simplest form, can be written as

$$(\mathbf{R}_m)_{ij} = \sum_{q=1}^{Q} I(\mathbf{p}_q)\, e^{-\mathrm{j}\,(\mathbf{z}_i - \mathbf{z}_j)^T \mathbf{p}_{m,q}},$$

where $(\mathbf{R}_m)_{ij}$ is the measured correlation between antennas i and j at STI interval m, $I(\cdot)$ is the brightness image (map) of interest, and $\mathbf{p}_q$ is the unit direction vector of the qth source at a fixed reference time. $I(\mathbf{p}_q)$ is thus equal to σ_q^2 in (2). It describes the relation between the observed visibilities and the desired source brightness distribution (intensities), and it has the form of a Fourier transform; it is known in radio astronomy as the Van Cittert-Zernike theorem [4], [7]. Image formation (mapmaking) is essentially the inversion of this relation. Unfortunately, we have only a finite set of observations, therefore we can only obtain a dirty image

$$\begin{aligned} I_D(\mathbf{p}) &:= \sum_{i,j,m} (\mathbf{R}_m)_{ij}\, e^{\mathrm{j}\,(\mathbf{z}_i - \mathbf{z}_j)^T \mathbf{p}} \\ &= \sum_{q} I(\mathbf{p}_q)\, B(\mathbf{p} - \mathbf{p}_q), \end{aligned}$$

where $\mathbf{p}$ corresponds to a pixel in the image, and where the dirty beam, also referred to as synthesized beam or point spread function (PSF), is given by

$$B(\mathbf{p} - \mathbf{p}_q) := \sum_{i,j,m} e^{\mathrm{j}\,(\mathbf{z}_i - \mathbf{z}_j)^T (\mathbf{p} - \mathbf{p}_{m,q})}.$$

$I_D(\mathbf{p})$ is the desired image convolved with the dirty beam, essentially a nonideal PSF due to the finite sample effect.

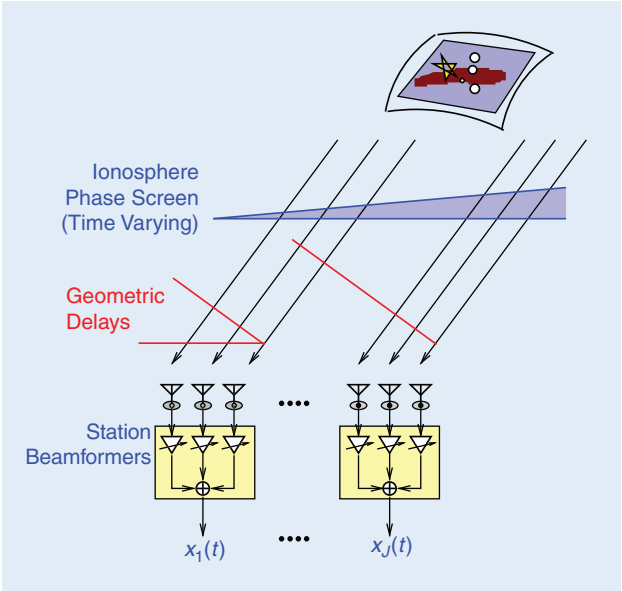

[FIG5] A radio interferometer where stations consisting of phased array elements replace telescope dishes. The ionosphere adds phase delays to the signal paths. If the ionospheric electron density has the form of a wedge, it will simply shift the apparent positions of all sources.

HIGH-RESOLUTION SYNTHESIS IMAGING WOULD NOT BE POSSIBLE WITHOUT ACCURATE CALIBRATION.

Every point source excites a beam $B(\cdot)$ centered at its location $\mathbf{p}_q$. Deconvolution is the process of recovering $I(\cdot)$ from $I_D(\cdot)$ using knowledge of the dirty beam. A standard algorithm for doing this is CLEAN [8]. The autocorrelations are often not used in the image formation process to reduce the impact of errors in the calibration of the additive noise on the resulting image. More details are shown in [9] and in the companion article [5].

NONIDEAL MEASUREMENTS

Although the previous equations suggest that it is rather straightforward to make an image from radio interferometer data, there are several effects that make matters more complicated.

- *Receiver element complex gain variations*. Astronomical signals are very weak, and radio telescopes therefore need to be very sensitive. This sensitivity is inversely proportional to the (thermal) noise. This dictates the use of low-noise amplifiers, which are sometimes even cryogenically cooled. Variations in environmental conditions of the receiver chain, such as temperature, cause amplitude and phase changes in the receiver response. Signals must also be propagated over long distances to a central processing facility and, depending on where digitization occurs, there can be significant phase and gain variations over time along these paths.
- *Instrumental response*. The sensitivity pattern of the individual elements, the primary beam, of an interferometer will never be perfect. Although it is steered towards the source of interest, the sensitivity in other directions (the side lobe response) on the sky will not be zero. This poses a challenge in the observation of very weak sources that may be hampered by signals from strong sources that are received via the side lobes but are still competing with the signal of interest. The algorithms correcting for the instrumental response assume that the sensitivity pattern is known. This may not be true with the desired accuracy if the array is not yet calibrated.
- *Propagation effects*. Ionospheric and tropospheric turbulence cause time-varying refraction and diffraction, which has a profound effect on the propagation of radio waves. As illustrated in Figure 5, in the simplest cases this leads to a shift in the apparent position of the sources. More generally, this leads to image distortions that are comparable to the distortions one sees when looking at lights from the bottom of a swimming pool.

In practice, $\mathbf{A}_m$ in (2) is thus corrupted by a complex gain matrix $\mathbf{G}_m$, which includes both source direction dependent perturbations and electronic instrumentation gain errors. It is the objective of calibration to estimate this matrix and track its changes over the duration of the observation. Some corrections (e.g., the complex antenna gain variations) can be applied directly to the measured correlation data, whereas other corrections (e.g., the propagation conditions) are direction-dependent and are incorporated in the subsequent

imaging algorithms. Very often, the estimation of the calibration parameters is done in an iterative loop that acts on the correlation (visibility) data and image data in turn, e.g., the self-calibration (Self-Cal) algorithm [10], [11] that is discussed in more detail later.

LOFAR IS A PHASED ARRAY WITH OVER 10,000 ANTENNAS.

TELESCOPE ARCHITECTURES

The physical model underlying the array calibration depends on the instrument architecture. This architecture also determines the capabilities of the telescope and may therefore have a profound effect on the calibration strategy, as we will see later on.

The WSRT and the VLA have been the workhorses of radio astronomy since the 1970s. Both telescopes are arrays of 25 m dishes. The size of a dish determines its beamwidth, or FOV, at a given wavelength, hence the size of the resulting image, while the spatial extent of the array determines the resolution within the FOV. The illumination pattern of the feed on each dish determines its sensitivity pattern, which is commonly referred to as the primary beam. These telescopes can also form an instantaneous beam within this primary beam by coherent addition of the telescope signals (beamforming). This beam is called the array beam. Visibilities are measured by correlating the telescope signals. The baseline vectors on which the visibility function is observed during a full observation describe a synthesized aperture. The sampling within this aperture determines the sensitivity pattern of the synthesis observation, which is referred to as the synthesized beam or PSF and corresponds to the dirty beam in the previous section. We thus have a beam hierarchy from the primary beam, which has a relatively large FOV (degrees) and relatively low sensitivity, via the instantaneously formed array beam to the PSF, which has a small FOV (arcsec) and a high sensitivity.

The WSRT and the VLA have their optimum sensitivity at frequencies of one to a few gigahertz. At lower frequencies, several things change. There are many stronger sources (e.g., synchrotron emission power is proportional to wavelength), thus even sources far outside the main beam of the PSF may show their effect due to nonideal spatial sampling. At low frequencies, the ionosphere is also much more variable (the phase delays are proportional to wavelength). Observations at these frequencies are therefore more challenging and require considerable processing power for proper calibration. High dynamic range imaging at these frequencies has therefore only recently been considered.

In the LOFAR [12], [13], which is currently being built in The Netherlands, the dishes are replaced by stations, each consisting of many small antennas distributed over an area of about 100×100 m. Some stations are very closely spaced, others are placed up to several 100 km away from the core. A station is a phased array of receiving elements with its own beamformer. The stations are steered electronically instead of mechanically, which allows them to respond quickly to transient phenomena. The receiving elements can either be individual antennas (dipoles), or compound elements (tiles) consisting of multiple antennas whose signals are combined using an analog beamformer. This system concept introduces two additional levels in the beam hierarchy: the compound (tile) beam and the station beam. The complete hierarchy of beam patterns is illustrated in Figure 3. The Murchison widefield array (MWA) has a similar design and purpose as LOFAR but is placed in the outback of Western Australia and has a maximum baseline length of about 3 km [14].

At first sight, there is not much difference between the calibration of an array of stations (or dishes) and the calibration of a station itself, but there are indeed some subtle differences. A station only contains short baselines ($\sim$100 m), which implies that it provides a much lower resolution than an array, while its constituents provide a much wider FOV. As we will see in the next section, this implies that the calibration becomes more challenging due to direction-dependent effects. Another challenging aspect stems from the enhanced flexibility of electronic beamforming: this may result in a less stable beam than a beam that is produced mechanically with a reflector dish. Finally, the output of a station beamformer is insufficient for calibration: for this purpose the station should also provide the correlation data among individual elements, even if these are not used at higher levels in the hierarchy.

A compound element (tile) can also be exploited as focal plane array (FPA). In this case, the array is placed in the focal plane of a dish. This allows to optimize the illumination of the dish, as it effectively defines a spatial taper over the aperture of the dish that can be used to create lower spatial side lobes. An FPA can also improve the FOV of the dish by providing multiple beams (off-axis) on the sky. In this case, the primary beam is the sensitivity pattern produced if the dish is illuminated by only a single antenna of the compound element. The compound beam is the electronically formed beam produced by illuminating the dish by the FPA. The FPA concept is currently under study in The Netherlands [15], United States [16], [17], and Australia [18] as part of the technology road map towards the SKA [19].

The SKA is a future telescope that is currently in the concept phase. It is a wide-band instrument that will cover the frequency range from 70 MHz to above 25 GHz. Apart from cost, the design is driven by a tradeoff between sensitivity and survey speed: the speed at which the complete sky can be observed. To enable wide-band operation, it will probably use a mix of the following receiver technologies:

- *Dishes with wide-band single pixel feeds*. This gives the highest sensitivity at the highest frequencies. Since this concept provides a very stable beam, it is well suited for high-fidelity imaging.
- *Dishes with FPAs*. At intermediate frequencies, FPAs can be used to enlarge the FOV of a single dish in a cost-effective way.

■ *Aperture arrays*. At low frequencies, it is easier to obtain a large collecting area, hence sensitivity, by using dipoles instead of dishes. Aperture arrays have the additional advantage of being very flexible: by duplicating the receiver chains one can have multiple independent beams on the sky, bandwidth can be traded against the number of beams on the sky, and electronic beamforming provides a quick response time to transient events.

The configuration of the SKA is still under study. Current concepts include a dense core that contains, e.g., half of all receivers within a diameter of 5 km, stations consisting of aperture arrays out to a maximum baseline of 180 km, and dishes out to a maximum baseline of 3,000 km.

CALIBRATION SCENARIOS

In the previous section, we introduced several telescope architectures, each with different characteristics, hierarchy, and parameterizations of the observed data model. This will lead to a wide variety of calibration requirements and approaches. Fortunately, it is possible to discuss this in a more structured manner by using only four different scenarios [20], each of which can be described by a distinct specialization of the measurement equation [21]. Each scenario considers the calibration of an array of elements with complex gain variations and spatially varying propagation effects. The scenarios compare the array aperture (the length of the largest baseline) to the FOV (the beamwidth of each individual array element) and the isoplanatic patch size, i.e., the scale at which the ionosphere/troposphere can be considered constant.

SCENARIO 1

As shown in Figure 6(a), the receiving elements of the array have a small FOV, and the maximum baseline is short. In this case, all receiving elements and all lines of sight within the FOV experience the same propagation conditions: the

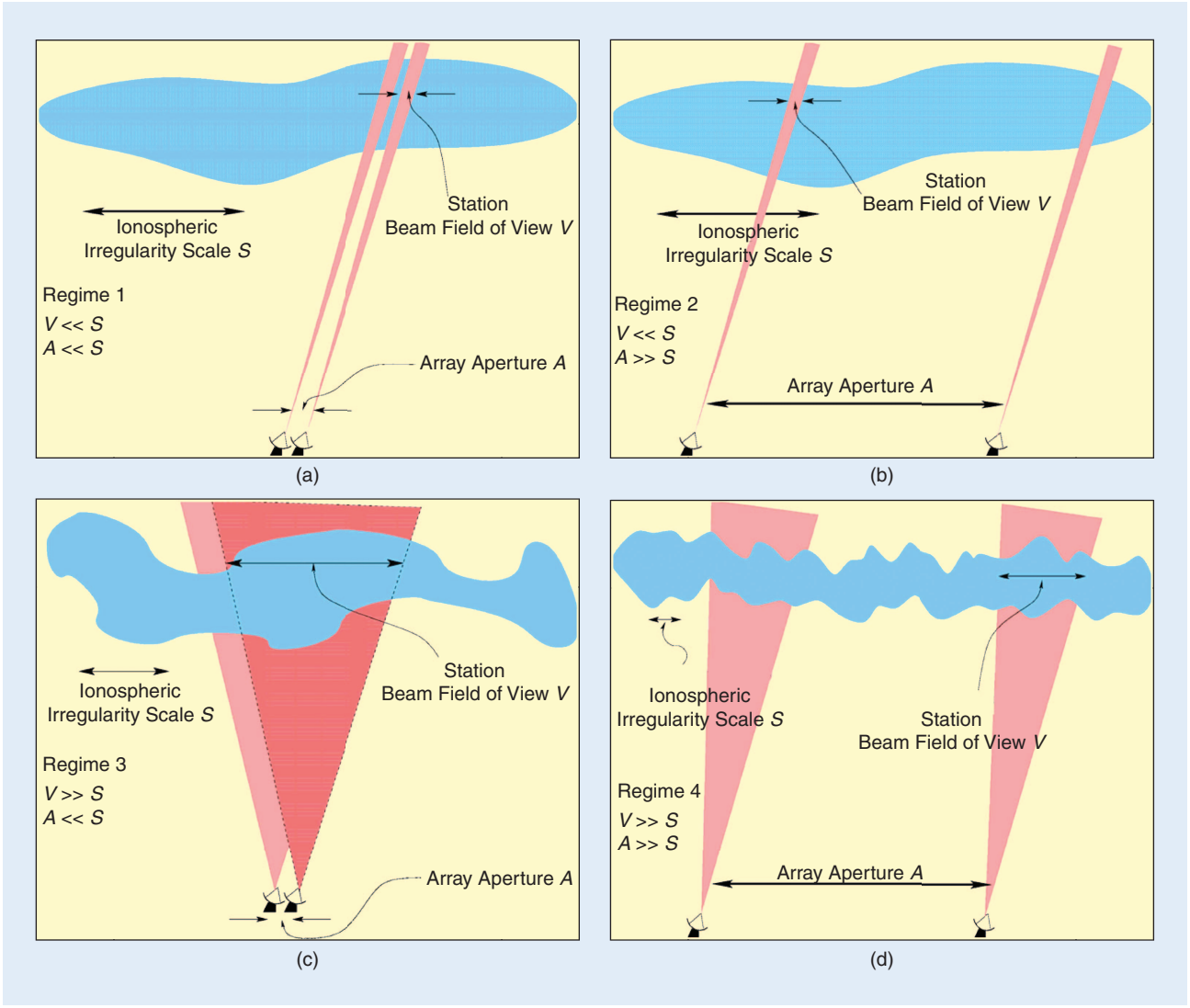

[FIG6] Calibration scenarios 1–4 are shown in (a)–(d) as defined by Lonsdale [20].

propagation effects do not distort the image. This scenario represents the case in which direction-dependent effects do not play a significant role. The calibration routine can therefore focus completely on element based gain effects. Since the FOV is small, it is often possible to calibrate on a single strong source in the FOV, especially if the array elements can be steered to a nearby calibration source. Due to its simplicity, this scenario is often used to obtain a first-order calibration for new instruments.

IN SCENARIO 3, SOURCES MAY HAVE SHIFTED IN APPARENT LOCATION.

SCENARIO 2

In this scenario [Figure 6(b)], we have a large array consisting of elements with a small FOV. Lines of sight from different elements towards the region of interest are subject to different propagation conditions, but the propagation conditions for all lines of sight within the FOV of an individual element are the same. The propagation effects can therefore be merged with the unknown receiver gains of each element, and the array can be calibrated under the same assumptions as in the first scenario. This scenario is valid for most of the interferometers built in the 1970s and 1980s, such as the WSRT and the VLA, and for VLBI observations.

SCENARIO 3

Figure 6(c) depicts the third scenario in which the elements have a large FOV, but the array is small. This implies that all lines of sight go through the same propagation path, but that there may be considerable differences in propagation conditions towards distinct sources within the FOV. The ionosphere and troposphere thus impose a direction-dependent gain effect that is the same for all elements. This scenario can also handle instrumental effects that are the same for all elements (e.g., irregular antenna beamshapes) and is therefore well suited for the situation of a compact array of identical elements such as the MWA and a single LOFAR or SKA station.

SCENARIO 4

As shown in Figure 6(d), the elements have a large FOV and the array has a number of long baselines. The lines of sight towards each source may experience propagation conditions that differ for different elements in the array. This implies that distinct complex gain corrections may be required for each source and each receiving element. Calibration is not possible without further assumptions on stationarity over space, time, and/or frequency. This is the most general scenario, and valid for future telescopes such as LOFAR, SKA, and ALMA.

ARRAY CALIBRATION

SCENARIO 1

In Scenario 1, the FOV of each array element (dish) is small and it is reasonable to assume that there is only a single calibrator source within the beam. Often, the beam will even have to slightly point away from the field of interest to "catch" a nearby strong calibrator source. The calibrator should be unresolved, i.e., appear as a point source, as opposed to the extended structure visible in Figure 1.

We will assume that the STI sample covariance matrices $\hat{\mathbf{R}}_m$ are calibrated independently and omit the subscript m for notational convenience. Continuity over many STIs needs to be exploited under Scenario 4 and will thus be discussed later. The data model (measurement equation) under Scenario 1 is given by

$$\mathbf{R} = \mathbf{G}\mathbf{K}\,\Sigma_s\,\mathbf{K}^H\mathbf{G}^H + \Sigma_n, \tag{3}$$

where $\mathbf{G} = \mathrm{diag}(\mathbf{g})$ is a diagonal matrix. For a single calibrator source, $\mathbf{K}$ has only a single column representing the geometric phase delays of the array towards the source, and $\Sigma_s = \sigma_s^2$ is a scalar with the source power. Both the direction of the source and its power are known from tables. Thus, in essence the problem simplifies to

$$\mathbf{R} = \mathbf{g}\mathbf{g}^H + \Sigma_n.$$

This is recognized as a "rank-1 factor analysis" model in multivariate analysis theory [22], [23]. Given $\hat{\mathbf{R}}$, we can solve for $\mathbf{g}$ and Σ_n in several ways [24]–[26]. For example, any submatrix away from the diagonal is only dependent on $\mathbf{g}$ and is rank 1: this allows direct estimation of $\mathbf{g}$. In the more general case described by (3), multiple calibrators may be simultaneously present. The required multisource calibration is discussed in, e.g., [27]–[30].

SCENARIO 2

In this scenario, the ionospheric or tropospheric phases are different for each array element, but the FOV is narrow, and it is possible to assign the unknown ionospheric or tropospheric phases to the individual antennas. Thus, the problem reduces to that of Scenario 1, and the same calibration solution applies.

SCENARIO 3

This scenario is relevant for sufficiently compact arrays, e.g., the calibration of a SKA or LOFAR station or an array with a relatively small physical extent like the MWA. The phase and gain of the station beam FOV is direction-dependent but the array elements see the same ionosphere. It is possible to make a coherent image, but sources may have shifted to different locations.

Since the FOV is large, several calibrator sources (say Q) will be visible. The model given by (3) for Scenario 1 can be extended to include unknown source dependent complex gains

$$\mathbf{R} = (\mathbf{G}_1\mathbf{K}\mathbf{G}_2)\Sigma_s(\mathbf{G}_1\mathbf{K}\mathbf{G}_2)^H + \Sigma_n\,,$$

where $\mathbf{G}_1 = \mathrm{diag}(\mathbf{g}_1)$ represents the antenna gain, and $\mathbf{G}_2 = \mathrm{diag}(\mathbf{g}_2)$ the source dependent complex gains, which

describe the antenna beam shape and the propagation conditions. In this model, we can merge the unknown $\mathbf{G}_2$ with Σ_s to obtain a single unknown diagonal source matrix $\Sigma = \mathbf{G}_2 \Sigma_s \mathbf{G}_2^H$, i.e.,

$$\mathbf{R} = \mathbf{G}\mathbf{K}\,\Sigma\mathbf{K}^H\mathbf{G}^H + \Sigma_n.$$

Given $\mathbf{R}$, the objective is to estimate $\mathbf{G}$, Σ, and Σ_n. Here, $\mathbf{K}$ is known as we know the source locations. If there is significant refraction, each viewing direction may pass through a different phase wedge, causing direction dependent motion of sources (but no further deformation). In that case, we will also have to include a parametric model for $\mathbf{K}$ and solve for the source directions (DOA estimation). This scenario is treated in, e.g., [30] and [35].

The most straightforward algorithms to solve for the unknowns are based on alternating least squares. Assuming that a reasonably accurate starting point is available, we can solve $\mathbf{G}$, Σ and Σ_n in turn, keeping the other parameters fixed at their previous estimates [30].

- *Solve for instrument gains*

$$\begin{aligned}\hat{\mathbf{g}} &= \operatorname*{argmin}_{\mathbf{g}} \|\hat{\mathbf{R}} - \mathbf{G}(\mathbf{K}\,\Sigma\mathbf{K}^H)\mathbf{G}^H - \Sigma_n\|^2 \\ &= \operatorname*{argmin}_{\mathbf{g}} \|\mathrm{vec}(\hat{\mathbf{R}} - \Sigma_n) + \\ &\quad -\mathrm{diag}(\mathrm{vec}(\mathbf{R}_0))(\overline{\mathbf{g}} \otimes \mathbf{g})\|^2,\end{aligned}$$

where $\mathbf{R}_0 = \mathbf{K}\,\Sigma\,\mathbf{K}^H$. This problem cannot be solved in closed form. Alternatively, we can first solve an unstructured problem: define $\mathbf{v} = \overline{\mathbf{g}} \otimes \mathbf{g}$ and solve

$$\hat{\mathbf{v}} = \mathrm{diag}(\mathrm{vec}(\mathbf{R}_0))^{-1}\mathrm{vec}(\hat{\mathbf{R}} - \Sigma_n)$$

or equivalently

$$\widehat{\mathbf{g}\mathbf{g}^H} = (\hat{\mathbf{R}} - \Sigma_n) \oslash \mathbf{R}_0,$$

where $\oslash$ denotes a point-wise division. After this, we can do a rank-1 approximation to find $\mathbf{g}$. The point-wise division can lead to noise enhancement; this is remediated by only using the result as initial estimate for, e.g., Gauss-Newton iteration [28] or by formulating a weighted least squares problem instead [26], [30].

- *Solve for source powers* $\sigma = \mathrm{diag}(\Sigma)$:

$$\begin{aligned}\hat{\sigma} &= \operatorname*{argmin}_{\sigma} \|\hat{\mathbf{R}} - \mathbf{G}\mathbf{K}\,\Sigma\mathbf{K}^H\mathbf{G}^H - \Sigma_n\|_F^2 \\ &= \operatorname*{argmin}_{\sigma} \|\mathrm{vec}((\hat{\mathbf{R}} - \Sigma_n) - (\mathbf{G}\mathbf{K})\Sigma(\mathbf{G}\mathbf{K})^H)\|^2 \\ &= \operatorname*{argmin}_{\sigma} \|\mathrm{vec}(\hat{\mathbf{R}} - \Sigma_n) - \overline{(\mathbf{G}\mathbf{K})} \circ (\mathbf{G}\mathbf{K})\sigma\|^2 \\ &= (\overline{\mathbf{G}\mathbf{K}} \circ \mathbf{G}\mathbf{K})^{\dagger}\mathrm{vec}(\hat{\mathbf{R}} - \Sigma_n).\end{aligned}$$

- *Solve for noise powers* $\sigma_n = \mathrm{diag}(\Sigma_n)$:

$$\begin{aligned}\hat{\sigma}_n &= \operatorname*{argmin}_{\sigma_n} \|\hat{\mathbf{R}} - \mathbf{G}\mathbf{K}\,\Sigma\mathbf{K}^H\mathbf{G}^H - \Sigma_n\|^2 \\ &= \mathrm{diag}(\hat{\mathbf{R}} - \mathbf{G}\mathbf{K}\,\Sigma\mathbf{K}^H\mathbf{G}^H).\end{aligned}$$

WITHOUT MAKING FURTHER ASSUMPTIONS, SCENARIO 4 IS NOT IDENTIFIABLE.

A more optimal solution can be found by covariance matching estimation, which provides an asymptotically unbiased and statistically efficient solution [36]. However, there is no guarantee that this will hold for a weighted alternating least squares approach. Fortunately, the simulations in [30] suggest that it does for this particular problem, even if the method is augmented with weighted subspace fitting [37], [38].

The first step of this algorithm is closely related to the SelfCal algorithm [10], [11] widely used in the radio astronomy literature, in particular for solving Scenarios 1 and 2. In this algorithm, $\mathbf{R}_0$ is a reference model, obtained from the best known map at that point in the iteration.

An alternative implementation is field-based calibration [39]. Assuming the instrumental gains have been corrected for, an image based on a short time interval is made. The apparent position shifts of the strongest sources are related to ionospheric phase gradients in the direction of each source. These "samples" of the ionosphere are interpolated to obtain a phase screen model over the entire FOV. This can be regarded as image plane calibration. The method is limited to the regime where the ionospheric phase can be described by a linear gradient over the array.

For the MWA, currently a real-time calibration method based on "peeling" is being investigated [40]. In this method of successive estimation and subtraction, calibration parameters are obtained for the brightest source in the field. The source is then removed from the data, and the process is repeated for the next brightest source. This leads to a collection of samples of the ionosphere, to which a model phase screen can be fitted.

SCENARIO 4

This scenario is the most general case and should be applied to large arrays with a wide FOV such as LOFAR and SKA. In this case, each station beam sees a multitude of sources, each distorted by different ionospheric gains and phases. The data model for the resulting direction-dependent calibration problem is

$$\mathbf{R} = \mathbf{A}\Sigma_s\mathbf{A}^H + \Sigma_n \;=\; (\mathbf{G} \odot \mathbf{K})\Sigma_s(\mathbf{G} \odot \mathbf{K})^H + \Sigma_n,$$

where $\mathbf{G} = [\mathbf{g}_1, \cdots, \mathbf{g}_Q]$ is now a full matrix, Σ_s and $\mathbf{K}$ are known, and $\mathbf{G}$ and Σ_n are unknown. Without making further assumptions, the solution is ambiguous: the gains are not identifiable.

This problem is discussed in [41] and studied in more detail in [42]. Possible assumptions that may lead to identifiability are listed next.

- *Bootstrapping from a compact core.* The planned geometry of LOFAR and SKA includes a central core of closely packed stations. Under suitable conditions, these can be calibrated as under Scenario 3, giving a starting point for the calibration of the other stations.

■ *Exploiting the different time and frequency scales.* Suppose we have a number of covariance observations $\mathbf{R}_{k,m}$, for different frequencies f_k and time intervals m. The matrix $\mathbf{K} = \mathbf{K}_{k,m}$ is varying over frequency and time, whereas the instrumental gains are relatively constant. This can be exploited to suppress contaminating sources by averaging over $\mathbf{K}_{k,m}$ while correcting the delays towards the calibrator sources.

■ *Modeling the gain matrix* $\mathbf{G} = \mathbf{G}_{k,m}$. The gain matrix can be approximated by a low-order polynomial model in k and m, leading to a reduction in the number of unknowns. As basis functions for the polynomials we can use the standard basis, or Zernike polynomials (often used in optics), or a Karhunen-Loeve basis derived from the predicted covariance matrix (see "Ionospheric Calibration Based on a Statistical Model").

THE MOST STRAIGHTFORWARD ALGORITHMS TO SOLVE FOR THE UNKNOWNS ARE BASED ON ALTERNATING LEAST SQUARES.

■ *Successive estimation and subtraction or "peeling."* In this method, a distinction is made between the instrumental gains and ionospheric gains based on considerations such as temporal stability and frequency dependence. Sources are estimated and removed from the data in an iterative manner.

IONOSPHERIC CALIBRATION BASED ON A STATISTICAL MODEL

Assume for simplicity a single calibration source at zenith. The data model is

$$\mathbf{R} = \mathbf{a}\mathbf{a}^H\sigma_s^2 + \sigma_n^2\mathbf{I},$$

where $\mathbf{a}$ is the spatial signature of the source at frequency f_k, as caused (only) by the ionosphere, and given by

$$\mathbf{a} = \exp(\mathrm{j}\boldsymbol{\phi}),\ \boldsymbol{\phi} = C\boldsymbol{\tau}f_k^{-1},$$

where $\boldsymbol{\phi}$ is a vector with J entries representing the ionospheric phases at each station, vector $\boldsymbol{\tau}$ contains the total electron content (TEC) seen by each station, and C is a constant. The TEC is the integral of the electron density along the line of sight, and is directly related to a propagation delay.

The ionosphere is often modeled as a turbulent slab of diffracting medium. Assuming a single layer and a pure Kolmogorov turbulence process, the covariance for $\boldsymbol{\tau}$ is modeled by a power law of the form

$$\mathbf{C}_\tau = \mathbf{I} - \alpha(\mathbf{D})^{\odot\beta}$$

with unknown parameters α and β (theoretically, $\beta = 5/3$ but measured values show that deviations are possible). The matrix $\mathbf{D}$ contains the pair-wise distances between all antennas, and is known.

Write the model as

$$\mathrm{vec}(\mathbf{R}) = (\bar{\mathbf{a}} \otimes \mathbf{a})\sigma_s^2 + \mathrm{vec}(\mathbf{I})\sigma_n^2.$$

The observed covariance matrix is $\mathrm{vec}(\hat{\mathbf{R}}) = \mathrm{vec}(\mathbf{R}(\boldsymbol{\tau})) + \mathbf{w}$, where the observation noise $\mathbf{w}$ has covariance $\mathbf{C}_\mathbf{w} = 1/\mathrm{N}(\mathbf{R}^T \otimes \mathbf{R})$. At this point, we could estimate τ by a least squares model matching. However, we have a priori knowledge on the parameters τ, i.e., the covariance $\mathbf{C}_\tau$. The maximum a posteriori (MAP) estimator exploits this knowledge, and leads to

$$\hat{\tau} = \arg\min_\tau \| \mathbf{C}_\mathbf{w}^{-\frac{1}{2}}\,\mathrm{vec}\,(\hat{\mathbf{R}} - \mathbf{R}(\boldsymbol{\tau}))\|^2 + \|\mathbf{C}_\tau^{-\frac{1}{2}}\tau\|^2.$$

This is solved as a nonlinear least squares problem (α and β are estimated as well).

The dimensionality can be reduced by introducing $\boldsymbol{\tau} = \mathbf{U}\boldsymbol{\theta}$, where $\mathbf{U}$ contains a reduced set of basis vectors. These can be

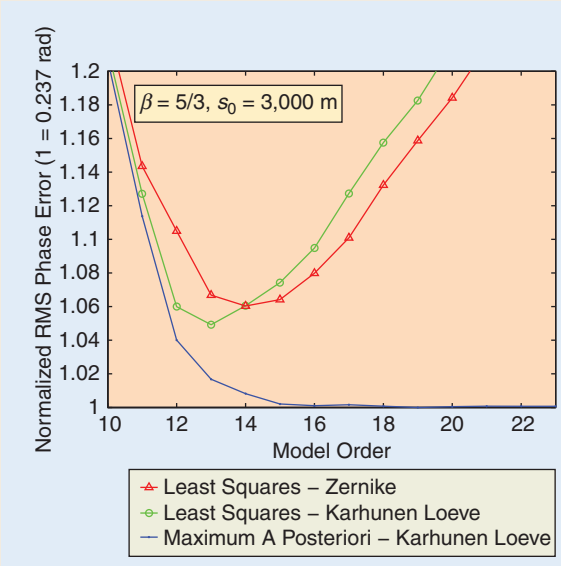

[FIGS1] Estimation performance as function of model order selection.

- data independent, e.g., simple polynomials, or Zernike polynomials [31]
- data dependent (Karhunen-Loeve), based on an eigenvalue decomposition of $\mathbf{C}_\tau$: $\mathbf{C}_\tau \approx \mathbf{U}\boldsymbol{\lambda}\mathbf{U}^H$. Only the dominant eigenvectors are retained.

The selection of the correct model order is often a tradeoff between reduced modeling error and increased estimation variance. Indeed, the simulation results shown in Figure S1 indicate that the least squares estimator (with either a Zernike basis or a Karhunen-Loeve basis) has an optimal model order, beyond which the mean squared estimation error increases. The MAP estimator adds an additional term to the cost function that penalizes "weak" parameters and makes it robust to overmodeling. For more details, see [32]. The validity of the turbulence model is experimentally tested on VLA survey data in [33] and [34].

This leads to a collection of samples to which a global model of the ionosphere or station beam can be fitted.

A complete calibration method that incorporates many of the above techniques was recently proposed in [43] and was successfully tested on a number of 74 MHz fields observed by the VLA. The behavior of this method at lower frequencies and/or on baselines longer than a few tens of kilometers still needs investigation.

FOR LOW-FREQUENCY INSTRUMENTS, IONOSPHERIC CALIBRATION IS A SIGNIFICANT CHALLENGE.

COMPOUND ELEMENT CALIBRATION

Compound elements are used in very large aperture arrays to keep the number of correlator inputs manageable, and FPAs to increase the FOV of dishes. In either case, each compound element produces a superposition of antenna signals, $\mathbf{x}(n)$, at its output port $y(n)$ during normal operation, i.e.,

$$y(n) = \mathbf{w}^H \mathbf{x}(n),$$

where $\mathbf{w}$ is the beamformer weight. Compound elements therefore require a separate calibration measurement before or after the observation, as only $y(n)$ is available and no antenna specific information can be derived from this superposition. Compound elements should thus be designed to be stable over the time scales of a typical observation.

Initial system characterization is often done in an anechoic chamber. In these measurements, the response $y(n)$ of the compound element to a test probe is recorded, while varying the beamformer weights $\mathbf{w}$ [44]. The measurements $y_1(n)$, $y_2(n), \ldots, y_N(n)$ are stacked in a vector $\mathbf{y}$ while the corresponding weights $\mathbf{w}_1, \mathbf{w}_2, \ldots, \mathbf{w}_N$ are stacked in a matrix $\mathbf{W}$. The complete series can be summarized as

$$\mathbf{y}(n) = \mathbf{W}^H \mathbf{G} \mathbf{k} s(n),$$

where $s(n)$ is the known input signal, $\mathbf{k}$ is the phase vector describing the geometrical delays due to the array and source geometry and $\mathbf{G} = \mathrm{diag}(\mathbf{g})$ contains the instrumental gains. The gains of the individual elements stacked in $\mathbf{g}$ are then easily derived. An attractive feature of this method is that it can also be used in the field using a stationary reference antenna [45].

Calibration of an aperture array of compound elements is discussed in the previous section. Regarding its use as an FPA in a dish, there are a number of differences, mostly because the dish projects an image of the sky within its FOV onto the FPA, whereas an aperture array measures the complex field distribution over the aperture itself.

The goal of FPA beamforming is to maximize the signal-to-noise ratio in an observation [16]. This involves a tradeoff between maximizing the gain in the direction of the source and minimization of the total noise in the system. A very intuitive approach to maximize the gain towards the source is conjugate field matching. For this calibration method, the array response $\mathbf{a}_p$ is measured for a strong point source for each of the P compound beams that will be formed by the FPA. The weights of the pth compound beam are chosen such that $\mathbf{w}_p = \mathbf{a}_p$. Since the dish forms an image of the point source on the FPA, most of the energy is concentrated on a few elements. Conjugate field matching thus assigns very high weights to a few elements and the noise of these elements will therefore dominate the noise in the observation. If one of these elements has a poor noise performance, conjugate field matching does not lead to the maximum signal-to-noise ratio in the observation. The measurement on a strong point source should therefore be augmented with a measurement on an empty sky to obtain the noise covariance matrix of the array. This step allows proper weighting of the receiver paths to optimize the signal-to-noise ratio of the actual observation. An excellent overview of FPA signal processing is provided in [17].

FUTURE CHALLENGES

Instruments like LOFAR and SKA will have an unprecedented sensitivity that is two orders of magnitude higher (in the final image) than current instruments can provide. The increased sensitivity and large spatial extent requires new calibration regimes, i.e., Scenarios 3 and 4, which are dominated by direction-dependent effects. Research in this area is ongoing. Although many ideas are being generated, only a limited number of new calibration approaches have actually been tested on real data. This is hardly surprising since only now the first of these new instruments are producing data. Processing real data will remain challenging and drive the research in this area of signal processing. Apart from the challenges discussed already throughout the text, some of the remaining challenges are as follows:

- *The sky.* Because of the long baselines that are part of the new instruments, many sources that appear point-like to existing instruments will be resolved. This means that they cannot be treated as point sources, but should be modeled as extended sources using, e.g., shapelets [46]. The new instruments will have wide frequency bands, so that the source structure may change over the observing band. For these reasons the source models will have to be more complicated than currently assumed. At the same time, due to the increased sensitivity, many more sources will be detected and will have to be processed. This will not only affect the calibration of the instruments but also the imaging and deconvolution.

  Because of their high sensitivity the new instruments are capable of detecting very weak sources, but they will have to do so in the presence of all the strong sources already known. Some of those strong sources may not even be in the FOV but may enter through the primary beam side lobes.
- *The instrument.* Both aperture arrays and dishes with FPAs have primary beams that are less stable than single pixel

primary beams from dishes. The primary beam is time dependent (if it is not fixed on the sky) and varies with frequency and over the different stations or FPA systems. These beam pattern variations have a negative impact on the achievable image quality. Calibrating for these beams is a real challenge, as is the correction for such beams during imaging.

- *The atmosphere*. For low-frequency instruments, ionospheric calibration is a significant challenge. Current algorithms have been shown to work for baselines up to about 30 km and frequencies as low as 74 MHz. However, for baselines of a few hundred up to a few thousand kilometers and frequencies down to, say, 10 MHz, these algorithms may not be valid.
- *Polarization purity*. Calibration and imaging have to take the full polarization of the signal into account. The primary beam of an instrument introduces instrumental polarization due to the reception properties of the feeds. If the feeds do not track the rotation of the sky, as is the case in any radio telescope that does not have an equatorial mount, the instrumental polarization varies over the observation. The ionosphere alters the polarization of the incoming electromagnetic waves as well due to Faraday rotation. These effects require calibration and correction with high accuracy.
- *The large number of elements*. Classical radio telescopes have (at most) an order of 60 receivers (WSRT has 14 dishes and the VLA has 27). Instruments like LOFAR, MWA, and the Electronic Multibeam Radio Astronomy Concept (EMBRACE) will have about 10^4 receiving elements while SKA is envisaged to have over 10^6 signal paths. The corresponding increase in data volumes will require sophisticated distributed signal processing schemes and algorithms that can run on suitable high-performance computing hardware.
- *Equations and unknowns*. It is clear that to deal with these challenges, more complicated models are needed, which in turn contain more unknowns that need to be extracted from the data. The increase in the number of stations will yield more equations, but this may not be enough. Modeling of the time-frequency dependence of parameters by a suitable set of basis functions will decrease the amount of unknowns that need fitting.
- *Interference mitigation*. The radio frequency spectrum is rather crowded, and it is expected that many observations will be contaminated by (weak or strong) radio frequency interference. Array signal processing techniques can be used to suppress interference, e.g., by active null steering or covariance matrix filtering [47], [48]. For LOFAR and SKA, no techniques have been proposed yet. Research from cognitive radio and compressive sensing may be very relevant for interference avoidance.

RESEARCH FROM COGNITIVE RADIO AND COMPRESSIVE SENSING MAY BE VERY RELEVANT FOR INTERFERENCE AVOIDANCE.

Finding suitable answers to these challenges will be of critical importance for the next generation of instruments.

ACKNOWLEDGMENTS

This work was supported in part by The Netherlands Organization for Scientific Research (NWO)-STW under grant DTC.5893. The Netherlands Institute for Research in Astronomy (ASTRON) is an institute of NWO.

AUTHORS

Stefan J. Wijnholds (wijnholds@astron.nl) received the M.Sc. degree in astronomy and the M.Eng. degree in applied physics (both cum laude) from the University of Groningen in 2003. After graduating, he joined The Netherlands Institute for Research in Astronomy (ASTRON) in Dwingeloo, where he works with the system design and integration group on the development of the next generation of radio telescopes. He has been with TU Delft, The Netherlands, since 2006, where he is pursuing a Ph.D. degree. His research interests lie in the area of array signal processing, specifically calibration and imaging.

Sebastiaan van der Tol (vdtol@strw.leidenuniv.nl) received the M.Sc. degree in electrical engineering from TU Delft, The Netherlands. In 2004, he became a research assistant with the same institute, where he is pursuing a Ph.D. degree in electrical engineering. Since 2009, he has been with Leiden University as a postdoctoral researcher. His current research interests include array signal processing and interference mitigation techniques for large phased array radio telescopes.

Ronald Nijboer (rnijboer@astron.nl) received the Ph.D. degree in 1998 from Vrije Universiteit, Amsterdam. From 1998 to 2004, he worked in the field of aeroacoustics with the National Aerospace Laboratory. In 2004, he started working for The Netherlands Institute for Research in Astronomy (ASTRON), where he leads the computing group. His research interests include calibration and imaging algorithms.

Alle-Jan van der Veen (a.j.vanderveen@tudelft.nl) received the Ph.D. degree (cum laude) from TU Delft in 1993. In 1994, he was a postdoctoral scholar at Stanford University. Currently, he is a full professor of digital signal processing at TU Delft. He received the 1994 and 1997 IEEE Signal Processing Society (SPS) Young Author Paper Award, and was an associate editor for *IEEE Transactions on Signal Processing*, chair of IEEE SPS Signal Processing for Communications Technical Committee, editor-in-chief of *IEEE Signal Processing Letters*, editor-in-chief of *IEEE Transactions on Signal Processing*, and member-at-large of the Board of Governors of IEEE SPS. He is currently a member of the IEEE SPS Awards Board and IEEE SPS Fellow Reference Committee. He is a Fellow of the IEEE.

REFERENCES

[1] Sloan Digital Sky Survey Home Page. [Online]. Available: http://www.sdss.org

[2] G. Battaglia, F. Fraternali, T. Oosterloo, and R. Sancisi, "HI study of the warped spiral galaxy NGC 5055: A disk/dark matter halo offset?" *Astron. Astrophys.*, vol. 447, pp. 49–62, Feb. 2006.

[3] M. Ryle, "A new radio interferometer and its application to the observation of weak stars," *Proc. Royal Soc. A*, vol. 211, no. 1106, pp. 351–375, 1952.

[4] A. R. Thompson, J. M. Moran, and G. W. Swenson, *Interferometry and Synthesis in Radio Astronomy*, 2nd ed. New York: Wiley, 2001.

[5] R. Levanda and A. Leshem, "Synthetic aperture radio telescopes," *IEEE Signal Processing Mag.*, vol. 27, no. 1, pp. 14–29, Jan. 2010.

[6] M. Zatman, "How narrow is narrowband," *IEE Proc. Radar, Sonar Navig.*, vol. 145, no. 2, pp. 85–91, Apr. 1998.

[7] R. A. Perley, F. R. Schwab, and A. H. Bridle, *Synthesis Imaging in Radio Astronomy (*Astron. Soc. Pacific Conf. Ser.*)*, vol. 6, San Francisco, CA: BookCrafters, 1994.

[8] J. A. Högbom, "Aperture synthesis with non-regular distribution of interferometer baselines," *Astron. Astrophys. Suppl.*, vol. 15, pp. 417–426, 1974.

[9] A. Leshem and A. J. van der Veen, "Radio-astronomical imaging in the presence of strong radio interference," *IEEE Trans. Inform. Theory*, vol. 46, no. 5, pp. 1730–1747, Aug. 2000.

[10] T. J. Cornwell and P. N. Wilkinson, "A new method for making maps with unstable radio interferometers," *Monthly Notices Royal Astron. Soc.*, vol. 196, pp. 1067–1086, 1981.

[11] T. J. Pearson and A. C. S. Readhead, "Image formation by self-calibration in radio astronomy," *Annu. Rev. Astron. Astrophys.*, vol. 22, pp. 97–130, Sept. 1984.

[12] J. D. Bregman, "Concept design for a low frequency array," in *SPIE Proc. Astronomical Telescopes and Instrumentation*, 2000, vol. 4015, pp. 19–33.

[13] M. de Vos, A. W. Gunst and R. Nijboer, "The LOFAR telescope: System architecture and signal processing," *Proc. IEEE,* vol. 97, no. 8, pp. 1431–1437, Aug. 2009.

[14] C. Lonsdale, "The Murchison widefield array," in *Proc. XXIXth General Assembly Int. Union of Radio Science (URSI GA)*, Chicago, IL, Aug. 7–16, 2008.

[15] W. A. van Cappellen, J. G. bij de Vaate, M. V. Ivashina, L. Bakker, and T. Oosterloo, "Focal plane arrays evolve," in *Proc. XXIXth General Assembly Int. Union of Radio Science (URSI GA)*, Chicago, IL, Aug. 7–16, 2008.

[16] K. F. Warnick and B. D. Jeffs, "Gain and aperture efficiency for a reflector antenna with an array feed," *IEEE Antennas Wireless Propagat. Lett.*, vol. 5, no. 1, pp. 499–502, Dec. 2006.

[17] B. D. Jeffs, K. F. Warnick, J. Landon, D. Jones, J. R. Fisher, and R. D. Norrod, "Signal processing for phased array feeds in radio astronomical telescopes," *IEEE J. Select. Top. Signal Process.*, vol. 2, no. 5, pp. 635–646, Oct. 2008.

[18] D. DeBoer, "Australian SKA Pathfinder," in *Proc. XXIXth General Assembly Int. Union of Radio Science (URSI GA)*, Chicago, IL, Aug. 7–16, 2008.

[19] P. J. Hall, "The square kilometer array: An international engineering perspective," *Exp. Astron.*, vol. 17, no. 1–3, pp. 5–16, 2004.

[20] C. Lonsdale, "Calibration approaches," MIT Haystack Observatory, Westford, MA, Tech. Rep. LFD memo 015, Dec. 8, 2004.

[21] J. Hamaker, J. Bregman, and R. Sault, "Understanding radio polarimetry—I. Mathematical foundations," *Astron. Astrophys. Suppl. Ser.*, vol. 117, pp. 137–147, May 1996.

[22] K. V. Mardia, J. T. Kent, and J. M. Bibby, *Multivariate Analysis*. San Diego, CA: Academic, 1979.

[23] D. N. Lawley and A. E. Maxwell, *Factor Analysis as a Statistical Method*. London, U.K.: Butterworth, 1971.

[24] A. J. Boonstra and A. J. van der Veen, "Gain calibration methods for radio telescope arrays," *IEEE Trans. Signal Process.*, vol. 51, no. 1, pp. 25–38, Jan. 2003.

[25] A. J. Boonstra, S. J. Wijnholds, S. van der Tol, and B. Jeffs, "Calibration, sensitivity and RFI mitigation requirements for LOFAR," in *IEEE Int. Conf. Acoustics, Speech Signal Processing (ICASSP)*, Philadelphia, PA, Mar. 18–23, 2005.

[26] S. J. Wijnholds and A. J. Boonstra, "A multisource calibration method for phased array telescopes," in *Proc. 4th IEEE Workshop on Sensor Array and Multi-channel Processing (SAM)*, Waltham, MA, July 2006, pp. 200–204.

[27] J. Pierre and M. Kaveh, "Experimental performance of calibration and direction finding algorithms," in *Proc. Int. Conf. Acoustics, Speech and Signal Processing (ICASSP'91)*, Toronto, Canada, May 1991, vol. 2, pp. 1365–1368.

[28] D. R. Fuhrmann, "Estimation of sensor gain and phase," *IEEE Trans. Signal Process.*, vol. 42, no. 1, pp. 77–87, Jan. 1994.

[29] B. P. Flanagan and K. L. Bell, "Array self calibration with large sensor position errors," *Signal Process.*, vol. 81, no. 10, pp. 2201–2214, Oct. 2001.

[30] S. J. Wijnholds and A. J. van der Veen, "Multisource self-calibration for sensor arrays," *IEEE Trans. Signal Process.*, vol. 57, no. 9, pp. 3512–3522, Sept. 2009.

[31] W. D. Cotton and J. J. Condon, "Calibration and imaging of 74 MHz data from the Very Large Array," in *Proc. XXVIIth General Assembly of the Int. Union of Radio Science (URSI)*, Maastricht, The Netherlands, Aug. 2002.

[32] S. van der Tol and A. J. van der Veen, "Ionospheric calibration for the LOFAR radio telescope," in *Proc. IEEE Int. Symp. Signals, Circuits, Systems*, Iasi, Romania, July 2007, pp. 457–460.

[33] A. S. Cohen and H. J. A. Röttgering, "Probing fine-scale ionospheric structure with the very large array radio telescope," *Astron. J*, vol. 138, no. 2, pp. 439–447, Aug. 2009.

[34] S. van der Tol, R. Sridharan, A. J. van der Veen, H. J. A. Röttgering, and A. S. Cohen, "Verification of an ionospheric turbulence model by VLA 74 MHz data," submitted for publication.

[35] A. J. Weiss and B. Friedlander, "'Almost Blind' signal estimation using second order moments," *IEE Proc. Radar, Sonar Navig.*, vol. 142, no. 5, pp. 213–217, Oct. 1995.

[36] B. Ottersten, P. Stoica, and R. Roy, "Covariance matching estimation techniques for array signal processing applications," *Digital Signal Process., Rev. J.*, vol. 8, pp. 185–210, July 1998.

[37] M. Viberg and B. Ottersten, "Sensor array processing based on subspace fitting," *IEEE Trans. Signal Process.*, vol. 39, no. 5, pp. 1110–1121, May 1991.

[38] M. Viberg, B. Ottersten, and T. Kailath, "Detection and estimation in sensor arrays using weighted subspace fitting," *IEEE Trans. Signal Process.*, vol. 39, no. 11, pp. 2436–2448, Nov. 1991.

[39] W. D. Cotton, J. J. Condon, R. A. Perley, N. Kassim, J. Lazio, A. S. Cohen, W. Lane, and W. C. Erickson, "Beyond the isoplanatic patch in the VLA Low-frequency Sky survey," in *Proc. SPIE*, Glasgow, Scotland, June 2004, vol. 5489, pp. 180–189.

[40] D. A. Mitchell, L. J. Greenhill, R. B. Wayth, R. J. Sault, C. J. Lonsdale, R. J. Cappallo, M. F. Morales, and S. M. Ord, "Real-time calibration of the Murchison widefield array," *IEEE J. Select. Top. Signal Process.*, vol. 2, no. 5, pp. 707–717, Oct. 2008.

[41] J. E. Noordam. (2002 Aug.). Generalized self-calibration for LOFAR, in *Proc. XXVIIth General Assembly of the International Union of Radio Science (URSI)*, Maastricht, The Netherlands [Online]. Available: http://www.ursi.org/Proceedings/ProcGA02/papers/1087.pdf

[42] S. van der Tol, B. D. Jeffs, and A. J. van der Veen, "Self-calibration for the LOFAR radio astronomical array," *IEEE Trans. Signal Process.*, vol. 55, no. 9, pp. 4497–4510, Sept. 2007.

[43] H. T. Intema, S. van der Tol, W. D. Cotton, A. S. Cohen, I. M. van Bemmel, and H. J. A. Röttgering, "Ionospheric calibration of low frequency radio interferometric observations using the peeling scheme. I. Method description and first results," *Astron. Astrophys.*, vol. 501, pp. 1185–1205, 2009.

[44] G. A. Hampson and A. B. Smolders, "A fast and accurate scheme for calibration of active phased array antennas," in *Proc. IEEE Antennas and Propagation Society Int. Symp.*, Orlando, FL, July 7–16, 1999, vol. 2, pp. 1040–1043.

[45] S. J. Wijnholds, "Evaluation and demonstration of THEP as a radio astronomical observing facility," M.S. thesis, Faculty of Natural Sciences, Univ. Groningen, Groningen, The Netherlands, 2003.

[46] A. Refregier, "Shapelets– I: A method for image analysis," *Monthly Notices Royal Astron. Soc.*, vol. 338, no. 1, pp. 35–47, 2003.

[47] A. Leshem and A. J. van der Veen, and A. J. Boonstra, "Multichannel interference mitigation techniques in radio astronomy," *Astrophys. J. Suppl.*, vol. 131, no. 1, pp. 355–374, Nov. 2000.

[48] A. J. van der Veen, A. Leshem, and A. J. Boonstra, "Signal processing for radio astronomical arrays," in *Proc. IEEE Sensor Array and Multichannel Signal Processing Workshop*, Sitges, Spain, July 2004, pp. 1–10. [SP]